Theoretical Explorations of Enantioselective Alkylation Reactions of Pyrroles and Indoles Organocatalyzed by Chiral Imidazolidinones

Ruth Gordillo, Jennifer Carter, K. N. Houk*

Department of Chemistry and Biochemistry University of California at Los Angeles, Los Angeles, CA 90095-1569, USA
Fax: (+1)-310-206-1843, e-mail: houk@chem.ucla.edu

Received: April 13, 2004; Accepted: July 30, 2004

Dedicated to the memory of Anne Giese-Ghosez.

Supporting Information for this article is available on the WWW under http://asc.wiley-vch.de/home/.

Abstract: The transition structures for MacMillan's alkylations of *N*-methylpyrrole by aldehydes catalyzed by chiral amine salts were explored with B3LYP/6-31G(d) density functional theory. These results provide an explanation of the enantioselectivities observed with these two catalysts.

Keywords: alkylation reactions; chiral imidazolidinones; enantioselection; hybrid density functional theory; organic catalysis

Introduction

Friedel–Crafts alkylations catalyzed by metal halides have been employed as a powerful C–C bond forming tool.[1] Only a few examples of an asymmetric version of this reaction are reported in the literature,[2] despite the chemical utility of the resulting compounds.

MacMillan et al. have developed several chiral organic amines that are organocatalysts for transformations typically carried out using metal salts as Lewis acids.[3–11]

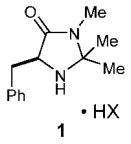

1

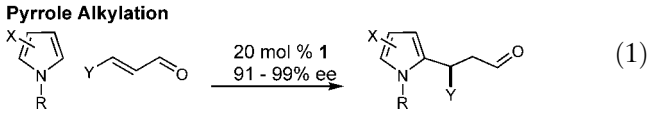

(1)

Organocatalyst **1** was investigated for the alkylations of pyrroles by α,β-unsaturated aldehydes as the electrophiles [Equation (1)].[5] Although electron-rich aromatics typically undergo 1,2-carbonyl addition, the iminium ions derived from **1** are inert to the 1,2-pathway based on steric constraints imposed by the catalyst framework. The heteroaromatic nucleophiles react *via* the less sterically demanding 1,4-addition pathway (Scheme 1). With TFA as the co-catalyst, 89–97% ees were achieved with a range of substituted pyrroles (R^1 = Me, Bn, allyl). In addition, 87–93% ees were obtained with alkyl, aromatic, or electron-withdrawing substituents on the α,β-unsaturated aldehydes (R^2 = Me, *i*-Pr, Ph, Bn, CO_2Me).

Catalyst **1** gave poor rates and enantioselectivities in the reactions between *N*-methylindole and (*E*)-crotonaldehyde [56% ee, 85% yield, Equation (2)].[6] This prompted MacMillan et al. to identify the more reactive amine catalyst, **2**. They reasoned that **2** should exhibit higher iminium ion formation efficiency, since the reactive lone pair on nitrogen is not eclipsed by the neighboring CH_3 as with **1**. In addition, the chiral iminium ion formed with catalyst **2** allows the heteroaromatic nucleophile to approach on the *Si,Re* face without steric obstruction. The (*E*) isomer of the iminium ion should

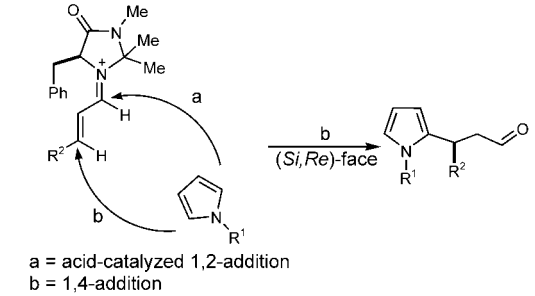

Scheme 1.

 DOI: 10.1002/adsc.200404107

also be preferred to minimize interactions with the *t*-butyl group. Indeed, improved yields were observed with various aldehydes (74–89%) and indoles (70–94%). The stereoselectivity also improved [89–97% ee, Equation (2)].[6]

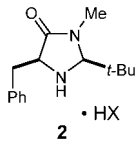

2

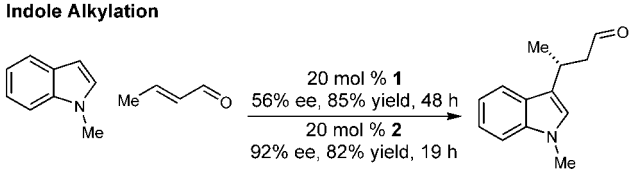

(2)

Alkylation reactions of pyrroles and indoles using chiral amines as organocatalysts constitute one example of general principle that MacMillan and coworkers have used for a wide range of reactions such as Diels–Alder cycloadditions,[3,8] 1,3-dipolar cycloadditions of nitrones,[4] the Mukaiyama–Michael reaction of silyloxyfurans with α,β-unsaturated aldehydes,[9] the 1,4-addition of electron-rich benzenes to α,β-unsaturated aldehydes,[7] α-oxidation of aldehydes,[10] and the α-chlorination of aldehydes.[11]

The condensation of an aldehyde with a chiral amine leads to the formation of an iminium intermediate. The energy of the LUMO on the carbonyl compound is lowered and the aldehyde is activated as an electrophile and dienophile. The product can be hydrolyzed to yield the enantioenriched product and regenerates the chiral amine catalyst (Scheme 2).

The ideal catalyst framework selectively forms one isomer of the iminium ion and shields one of the enantiofaces of the dienophile from the diene. MacMillan's explanations for the observed reactivity and enantioselectivity of these amine-catalyzed reactions were based on a model of the iminium ion **3** calculated with MM3, shown in Figure 1.[3,12] The (*E*)-iminium isomer was assumed to minimize non-bonding interactions between the substrate olefin and the geminal methyl substituents on the catalyst framework. In addition, the benzyl group attached to C5 of the imidazolidinone heterocycle was presumed to effectively shield the *Re,Si* face of the C=C double bond of the iminium ion. This has served as the model to rationalize the stereocontrol of reactions involving the intermediacy of **3**.

We have explored theoretically the alkylation reaction between *N*-methylpyrrole and (*E*)-crotonaldehyde catalyzed by chiral imidazolidinones **1** and **2**. The results can also be employed to explain the enantioselectivities for reactions of *N*-methylindole. The latter was computationally much more expensive, and only a few model calculations are reported for this large system.[6] Hybrid density functional theory was used in these studies.[13] This has been demonstrated to be a powerful tool to predict enantioselectivities in other asymmetric organocatalyzed reactions.[14]

Computational Methods

All structures were computed using the functional B3LYP[13a–c] and the 6–31G(d)[13d–f] basis sets as implemented in Gaussian 98.[15] All energy minima and transition structures were characterized by frequency analysis. Because of the high cost of the calculations, in the case of the calculated transition structures for the alkylation reaction of *N*-methylpyrrole with (*E*)-crotonaldehyde, only frequency calculations of the most stable transition structures were performed. Reported energies are electronic energies plus zero point vibrational energy corrections, scaled by 0.9806.[16] Cartesian coordinates of all reported structures as well as their computed total electronic energies are included in the Supporting Information. The energies computed for structures

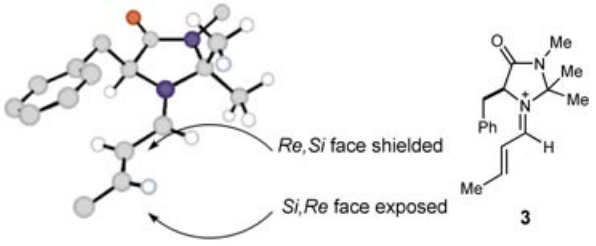

Figure 1. Computed MM structures of the iminium ion derived from imidazolidinone **1** and (*E*)-crotonaldehyde.[12]

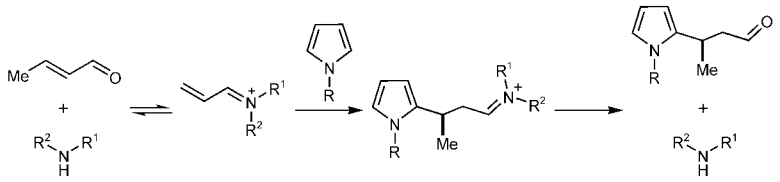

Scheme 2.

in solvent (water) include the electronic energy plus the solvation free energy from the CPCM solvation model.[17]

Results and Discussion

Conformational Study of the Iminium Complexes

There are six different conformations expected for the iminium intermediate **3**. These involve the (*E*) and (*Z*) configurations about the N^+=C bond and the three staggered conformations involving the bond to the benzyl group. Figure 2 shows the five energy minima that were found after optimization.

Contrary to previous force field energy minimizations,[3,18] conformer (*E*)-**3a**, which includes a stabilizing C–H···π interaction between one of the methyl groups at position C2 of the imidazolidinone ring, and the phenyl ring of the benzyl group at position C5, was found to be the global minimum. The distance between the carbon nucleus of the methyl group and the center of the aromatic ring is 3.8 Å. Tsuzuki et al. previously studied a benzene-methane complex at the MP2/cc-pVTZ level, and found an optimum C–Ar distance of 3.8 Å and stabilization of the complex of 1.5 kcal/mol.[19] Isomer (*E*)-**3b** is only 0.3 kcal/mol higher in energy than (*E*)-**3a**, and is quite similar to the structure found by MacMillan and coworkers based on MM calculations for iminium complex **3** (Figure 1).[3] Recently reported calculations of small hydrocarbon molecules show that a large basis set including multiple polarization functions and appropriate electron correlation correction are necessary to accurately evaluate C–H···π interaction energies.[20] Due to the large number of atoms in structures (*E*)-**3a** and (*E*)-**3b**, calculations involving the second-order Møller–Pleset perturbation method (MP2) were not carried out.[21] In order to prove the existence of such C–H···π stabilizing interaction in (*E*)-isomer **3a**, we have performed B3LYP single point calculations using the 6–311G(d, p) and the 6–311+G(d, p) basis sets for iminium ions (*E*)-**3a** and (*E*)-**3b**.[22,23] B3LYP/6-311G(d, p)//B3LYP/6-31G(d) and B3LYP/6-311+G(d, p)//B3LYP/6-31G(d) electronic energies were found to be 0.5 and 0.2 kcal/mol lower for structure (*E*)-**3a**. With the aim to check the solvent influence, we have also performed single point calculations for the most stable isomer (*E*)-**3a** and (*E*)-**3b**, using the solvation model CPCM (water ε = 78.39).[17] In water, the relative energy difference was strongly increased, (*E*)-**3b** being 1.7 kcal/mol higher in energy than (*E*)-**3a**.

The least stable (*E*)-isomer, (E)-**3c**, possesses a C–C bond to the phenyl ring, that is nearly eclipsed with the adjacent C–H bond of the iminium ring (H–C–C–Ph dihedral angle = 10.1^0). Surprisingly, a staggered conformer analogous to structure (*E*)-**3d** (Figure 3), could not be located. To compare the relative energies, conformer (*E*)-**3d** with the dihedral angle H–C–C–Ph constrained at -63.8^0 was also calculated. (*E*)-**3d** was found to be 3.5 kcal/mol higher in energy than the most stable (*E*)-isomer **3a**. The molecular electrostatic potential (MEP) analysis of the structure shows that the carbonyl oxygen and the phenyl ring are very close (Figure 3). Both of these have negative electrostatic potentials and are repulsive, forcing the normally favored staggered arrangement to rotate to eclipsed.

As summarized in Table 1, in general, (Z)-isomers are less stable than the analogous (*E*)-conformers. In the

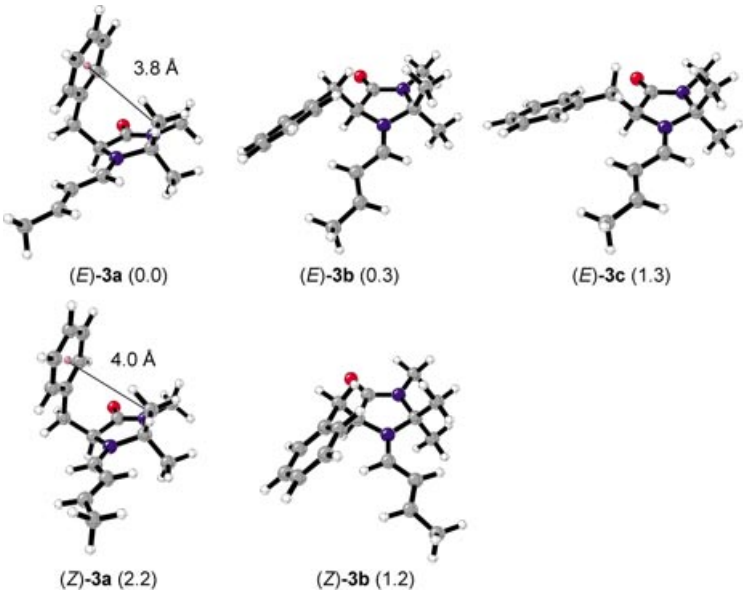

Figure 2. Optimized geometries and relative energies (kcal/mol in parenthesis) for the (*E*)-**3a** – (*E*)-**4c**, and (*Z*)-configurations **3a** and **3b** of the iminium formed from catalyst **1** and (*E*)-crotonaldehyde.

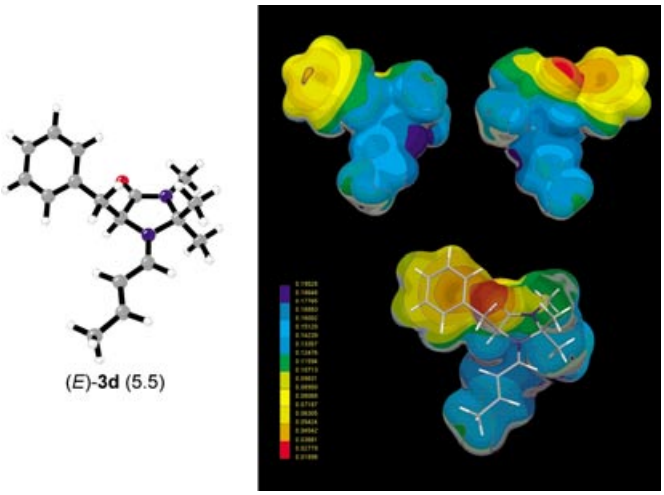

Figure 3. MEP of structure (*E*)-**3d** plotted onto a isodensity molecular surface (0.002 e au^{-13}).

case of the (*Z*)-iminium intermediates, higher steric hindrance between the two methyl groups at C2 of the imidazolidinone ring and the substituent attached to N1 destabilizes these structures. A conformer of the (*Z*)-isomer analogous to (*E*)-**3c** could not be found. The structure (*Z*)-**3c**, which is 5.5 kcal/mol higher in energy than (*E*)-**3a**, presented a negative frequency at $-9\,cm^{-1}$. The most stable iminium ions (*E*)-**3a** and (*E*)-**3b** are predicted to constitute 85% of all the possible species in the gas phase at 25 °C, and 93% in the gas phase at −60 °C (Table 1).

However, in contrast to previous surmise,[3,18] the (*Z*)-isomer **3b** was found to be close enough in energy to be considered for further transition structure searching.[5,6]

MacMillan et al. determined that replacing the *gem*-dimethyl substituents on the chiral amine catalyst with a *t*-butyl group led to increased stereoselectivity of the Friedel–Crafts reaction.[6] In order to account for the differences in stereoselectivity between the two catalysts the preferred conformations of iminium ion intermediate **4** were also studied (Figure 4). The most stable isomer (*E*)-**4b** has a structure similar to that predicted geometry by MacMillan et al.[6]

As with **3**, (*Z*)-isomers **4a – c** are less stable than the analogous conformers *(E)*-**4a**, (*E*)-**4b**, and (*E*)-**4c** (Table 2), for steric reasons.

Relative energy differences between isomers are higher for iminium complexes **4** than for structures **3**. In the case of **4**, the most stable conformers (*E*)-**4b** and (*E*)-**4c** constitute 92% of all the existing species in the gas phase at 25 °C, and 96% in the gas phase at −60 °C (Table 2). This fact can explain qualitatively why higher enantioselectivities were observed in the case of addition reactions with α,β-unsaturated aldehydes catalyzed by imidazolidinone **2** [addition of *N*-methylindole to (*E*)-crotonaldehyde using imidazolidinone catalyst **1** gave 56% ee, while catalyst **2** gave 92%].[6] Structures (*E*)-**4a**, (*E*)-**4b**, (*E*)-**4c**, and (*Z*)-**4b** were included in the transition structure analysis.

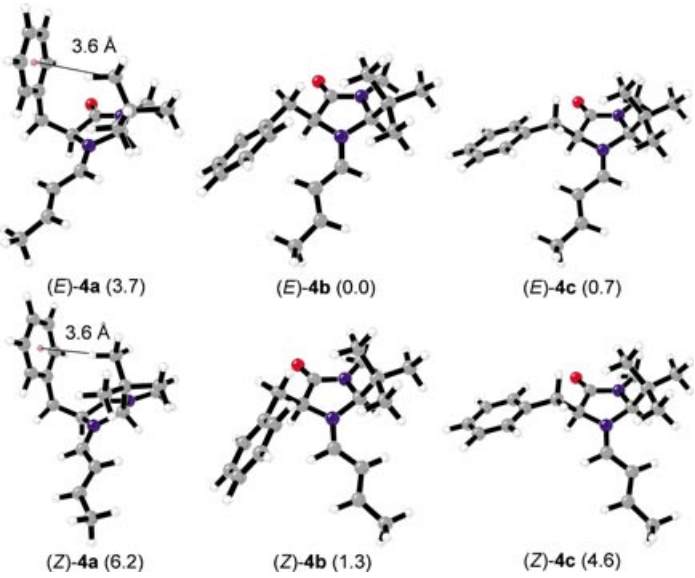

Figure 4. Optimized geometries and relative energies (kcal/mol) for the (*E*)-(**4a–4c**) and (*Z*)-(**4a–4c**) conformers of the iminium formed from catalyst **2** and (*E*)-crotonaldehyde.

Table 2. Percentage of each iminium complex **4** isomer in the gas phase at 25 °C and −60 °C.

Isomer	Relative Energy [kcal/mol]	Percent	
		25 °C	−60 °C
(*E*)-**4a**	3.7	0	0
(*E*)-**4b**	0.0	71	81
(*E*)-**4c**	0.7	21	15
(*Z*)-**4a**	6.2	0	0
(*Z*)-**4b**	1.3	8	4
(*Z*)-**4c**	4.6	0	0

Transition Structure Searching

Alkylation reactions described by MacMillan and coworkers represent common examples of electrophilic aromatic substitution on pyrroles and indoles.[5,6] The rate of the overall substitution is determined by attack of the electrophile, here the iminium ion, on the aromatic heterocycle to form a cationic species. This rapidly loses a proton to restore aromaticity and to form the products. It is widely known that in the case of pyrroles the substitution takes place at position C2 while indoles undergo electrophilic substitution at position 3.[24]

Table 1. Percentage of each iminium complex **3** isomer in the gas phase at 25 °C and −60 °C.

Isomer	Relative Energy [kcal/mol]	Percent	
		25 °C	−60 °C
(*E*)-**3a**	0.0	53	62
(*E*)-**3b**	0.3	32	31
(*E*)-**3c**	1.3	6	3
(*Z*)-**3a**	2.2	1	0
(*Z*)-**3b**	1.2	7	4

One important factor that determines efficiency of organocatalysts employed by MacMillan and coworkers in a wide range of asymmetric enantioselective reactions[3–11] is the reversible formation of iminium ions from chiral imidazolidinones and α,β-unsaturated carbonyl compounds. Finally, according to the reported experimental procedures, hydrolysis to the final products occurs smoothly, and does not have any influence in the chiral center generated in the first step of the reaction.

Before performing transition structure searching on the whole system, we explored all the possible approaches of the pyrrole and the indole rings to a model

iminium formed from dimethylamine and (*E*)-crotonaldehyde (Scheme 3).

The *s-cis* conformer of the dimethylamine-(*E*)-crotonaldehyde iminium complex is 6.6 kcal/mol higher in energy than the *s-trans*. Consequently, only the more stable *s-trans* isomer was included in the transition structure calculations (Scheme 4).

Four transition structures, **TS5** – **8**, were located for the alkylation reaction of pyrrole (Figure 5). The heterocycle can be directly above the alkene in a highly asynchronous Diels–Alder-like geometry (closed transition structures), or it can point away from the alkene (open transition structures). The pyrrole can also be oriented *endo* or *exo* to the iminium C=N$^+$ bond. The calculations show that the open structures, **TS7** and **TS8**, are more than 1 kcal/mol higher in energy than the closed structures, **TS5** and **TS6**. Thus, only the closed transition states were considered in the transition structure searches for the catalyzed alkylation reactions of *N*-methylpyrrole with (*E*)-crotonaldehyde. The closed transition structures resemble highly asynchronous Diels–Alder transition states. However, the transition vector for motion along the reaction coordinate corresponds to formation of the cation involving electrophilic attack on the pyrrole ring. The greater stability of the closed transition structures is most likely due to electrostatic stabilization of the developing partial charge on the pyrrole by the enamine π system.[25]

A similar study was carried out for the reaction of indole with (*E*)-crotonaldehyde catalyzed by dimethylamine. Only open structures could be located, and all attempts to locate closed structures were unsuccessful: transition state searches starting from structures analogous to **TS5** and **TS6** (Figure 5) optimized to open transition states **TS11 open3** and **TS12 open2** (Figure 6).

In Table 3 we display the calculated activation energies for pyrrole and indole alkylation reactions. Transition structures **TS9** – **TS11** have similar activation energies to the most unstable open transition structures in the case of pyrrole alkylation reaction, **TS7** and **TS8**. In the case of alkylation reactions catalyzed by amines **1** and **2**, transition structures similar to **TS11** and **TS12**, should be especially sensitive to steric hindrance produced by substituents at C2 and C5 of the imidazolidinone ring.

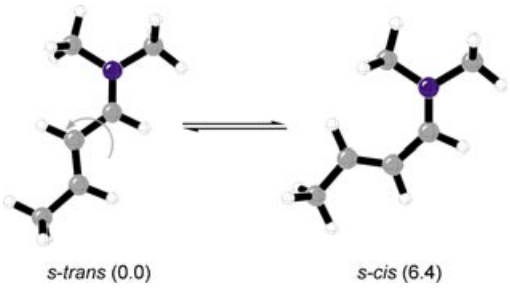

Scheme 4.

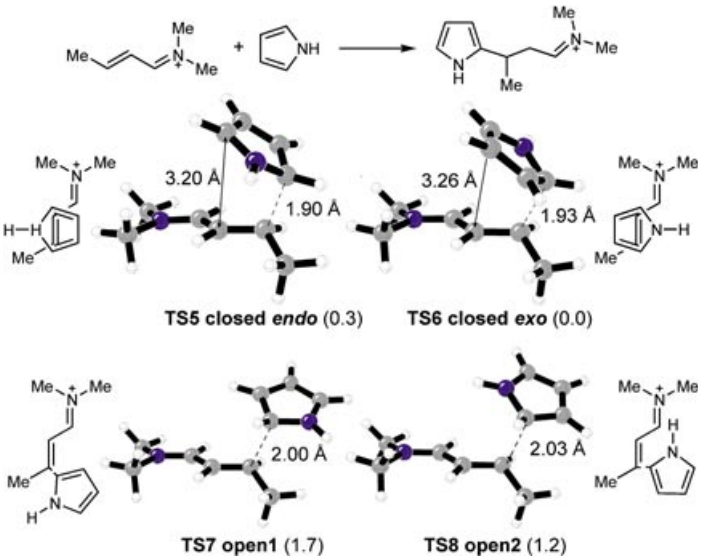

Figure 5. Optimized structures and relative energy differences of located closed and open transition structures of the alkylation reaction of pyrrole with (*E*)-crotonaldehyde catalyzed by dimethylamine.

The transition states for the reactions of *N*-methylpyrrole with iminium ions, and the alkylation products are shown schematically in Figure 7. Attack on the bottom face of the (*E*)-iminium intermediate, or on the top face of the (*Z*)-isomer (*Si*,*Re* face) gives the major product experimentally isolated. On the contrary, attack on the top face of the (*E*)-isomer, or on the bottom face of the (*Z*)-iminium complex (*Re*,*Si* face) forms the enantiomeric compound.

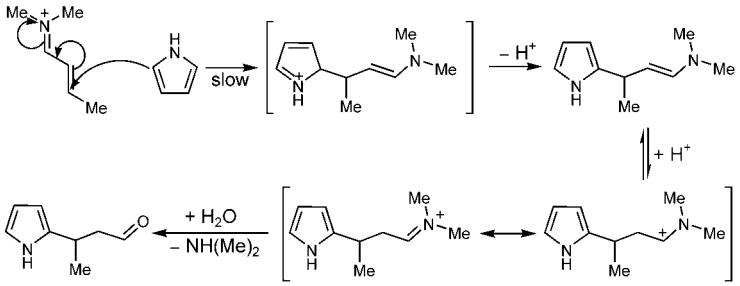

Scheme 3.

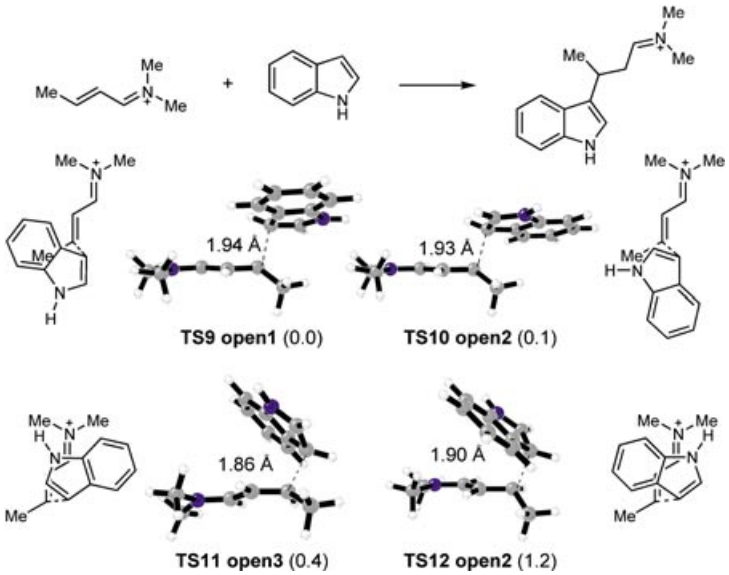

Figure 6. Optimized structures and relative energy differences of located open transition structures of the alkylation reaction of indole with (*E*)-crotonaldehyde catalyzed by dimethylamine.

Table 3. Calculated electronic activation energies of located transition structures of the alkylation reactions of pyrrole (**TS5** – **TS8**) and indole (**TS9** – **TS12**) with (*E*)-crotonaldehyde.

Transition Structure	$\Delta E^{\ddagger}$ [kcal/mol]
TS5 closed *endo*	5.1
TS6 closed *exo*	5.5
TS7 open1	6.3
TS8 open2	6.8
TS9 open1	6.5
TS10 open2	6.6
TS11 open3	6.9
TS12 open4	7.7

The lowest energy optimized transition structures for the reaction between *N*-methylpyrrole and the iminium ion intermediate derived from *trans*-2-butenal and **2** are shown in Figures 8 and 9. **TS13** – **TS15** correspond to the transition structures for attack of *N*-methylpyrrole on the *Si*,*Re* face of the iminium intermediate **3** (Figure 8). The *N*-methylpyrrole is in the closed position and *exo* in each case. The order of relative energies of the closed-*exo*-(*Si*,*Re*) transition structures differs from the order of the relative energies of iminium ion intermediate conformers **3** (Figure 2). **TS13** is lowest in energy, while **TS14**, favored by MacMillan et al.'s MM3 analysis[3] is 1.3 kcal/mol higher in energy. **TS15** is intermediate in energy. For reactions at $-60\,^{\circ}C$, the **TS13** will be the predominant transition structure leading to the major product formed experimentally.

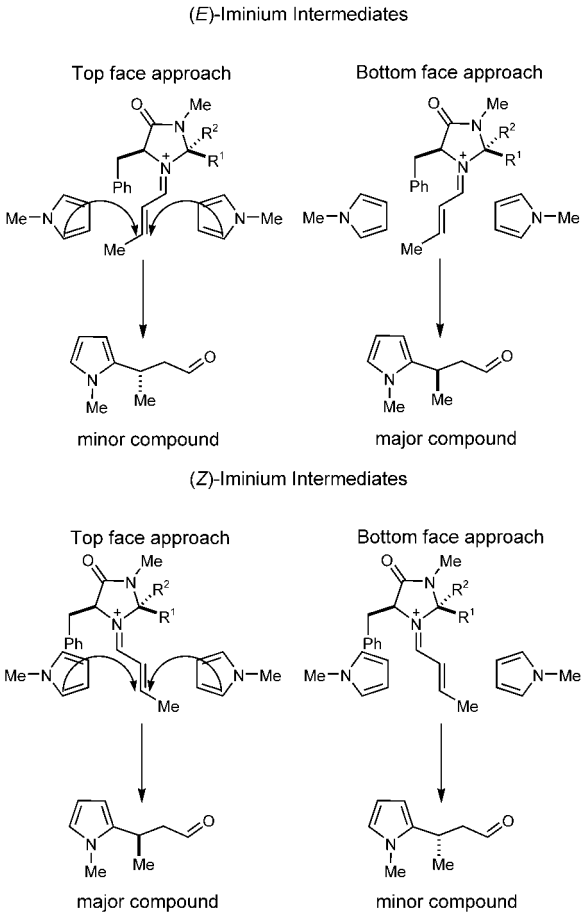

Figure 7. Modes of attack and products produced from the reaction of *N*-methylpyrrole and (*E*)-crotonaldehyde catalyzed by chiral imidazolidinones.

TS16 – **TS18** are the most stable closed-*endo*-(*Si*,*Re*) transition structures, which also give the product isolated as major compound (Figure 8). The conformations of the benzyl group in **TS16** – **TS18** are the same as the three low energy conformation of (*E*)-**3** (Figure 2). **TS16** is only 0.4 kcal/mol higher in energy than the corresponding *exo*-**TS13**, while **TS17** and **TS18** are slightly lower in energy in the corresponding closed-*exo* transition structures.

For comparison, Figure 9 shows the most stable calculated closed-*exo*- and closed-*endo*-(*Re*,*Si*) approaches of the pyrrole heterocycle to iminium conformers **3**. **TS19** is only 0.8 kcal/mol higher in energy than attack on the *Si*,*Re* face (**TS13**, Figure 8) and is actually lower in energy than attack on the *Si*,*Re* face for conformers **TS14** and **TS15**. Attack on the *Re*,*Si* face of eclipsed conformer **TS20** is 0.7 kcal/mol higher than *Si*,*Re* face attack. The orientation of the phenyl ring in conformer (*E*)-**3b** effectively prevents attack on the *Re*,*Si* face, as can be observed from data listed in Table 4.

Transition structures **TS22** – **TS24** result from the approaching of *N*-methylpyrrole to the *Re*,*Si* face of iminium intermediate **3**. Here, the heterocycle adopts an *endo*

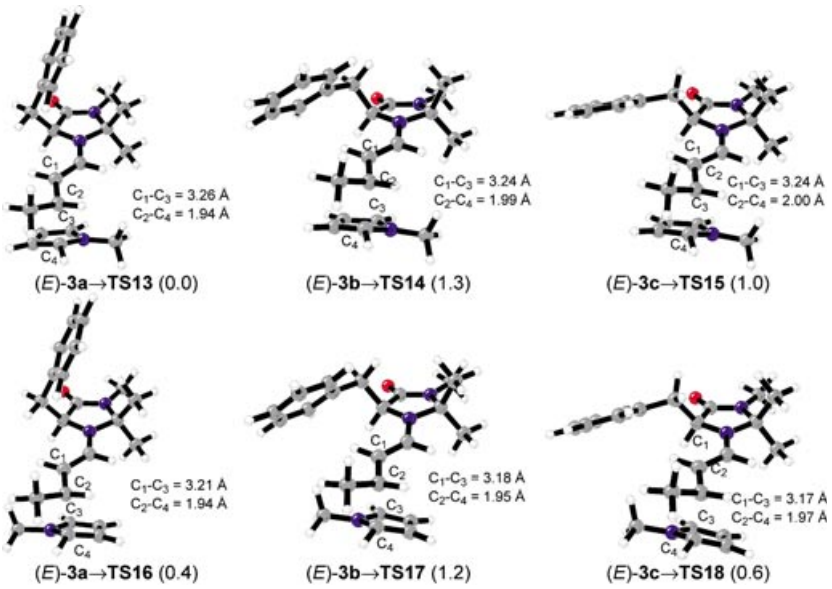

Figure 8. Optimized structures, relevant distances and relative energy difference for the most stable transition structures corresponding to *N*-methylpyrrole approach on the *exo*- and *endo*-(*Si*,*Re*)-face of iminium complex **3**.

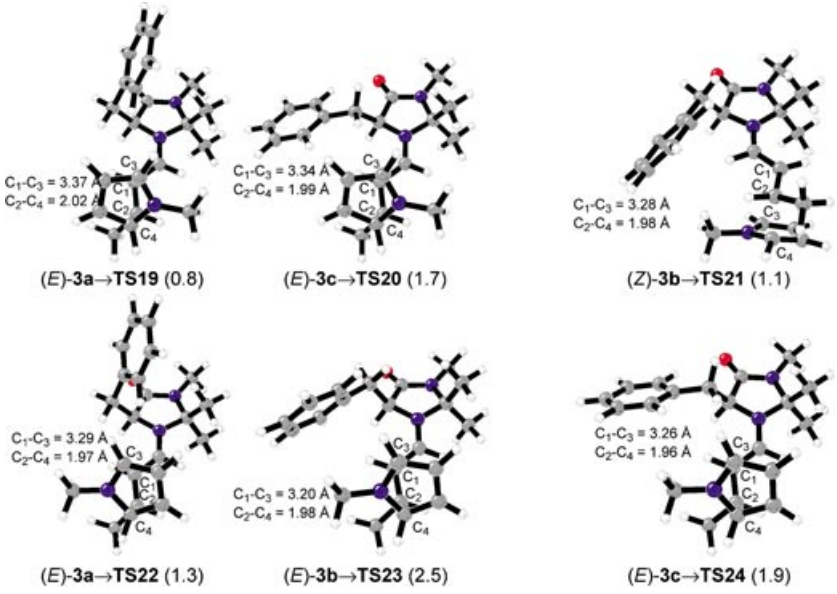

Figure 9. Optimized structures, relevant distances and relative energy difference for the most stable transition structures corresponding to *N*-methylpyrrole approach on the *exo*- and *endo*-(*Re*,*Si*)-face of iminium complex **3**.

orientation with respect to the C=N$^+$ bond. **TS22** and **TS24** represent the highest transition structures for conformers (*E*)-**3a** and (*E*)-**3c** respectively. **TS23**, with the phenyl ring over the reactive site, is effectively shielded for *Re*,*Si* attack. Closed-*exo*-(*Si*,*Re*), closed-*endo*-(*Si*,*Re*), and closed-*endo*-(*Re*,*Si*) approaches to iminium intermediate (*Z*)-**3b** are the least stable (2.4, 3.7, and 2.6 kcal/mol higher in energy than **TS13**, respectively) (Table 4).

A Boltzmann distribution was performed to determine the product ratio predicted from all these transition states (Table 4). A theoretical ee value of 71% is obtained at $-60\,^{\circ}C$ in the gas phase, close to the experimental value of 91%.[5] The calculated difference in activation free energies between the two products is 0.5 kcal/mol lower than observed experimentally. The calculated ratio of closed-*exo*:closed-*endo* transition states is 64:36.

MacMillan et al. observed improved enantioselectivities with catalyst **2** for the reaction between iminium ion intermediate **4** and *N*-methyl pyrrole.[6] The most stable calculated transition structures for the closed-*exo* and closed-*endo* orientations on the *Si*,*Re* and *Re*,*Si* faces of the iminium ion are shown in Figures 10 and 11.

Table 4. Percentage of transition structures **TS13** – **TS28** in the gas phase at $-60\,^{\circ}C$.

Approach	Iminium Ion	Relative Energy [kcal/mol]	Percent
exo-(*Si*,*Re*)	(*E*)-**3a**	0.0	45
	(*E*)-**3b**	1.3	2
	(*E*)-**3c**	1.0	4
	(*Z*)-**3b**	2.4	0
endo-(*Si*,*Re*)	(*E*)-**3a**	0.4	18
	(*E*)-**3b**	1.2	3
	(*E*)-**3c**	0.6	12
	(*Z*)-**3b**	3.7	0
exo-(*Re*,*Si*)	(*E*)-**3a**	0.8	7
	(*E*)-**3b**	3.4	0
	(*E*)-**3c**	1.7	1
	(*Z*)-**3b**	1.1	4
endo-(*Re*,*Si*)	(*E*)-**3a**	1.3	2
	(*E*)-**3b**	2.5	0
	(*E*)-**3c**	1.9	1
	(*Z*)-**3b**	2.6	0

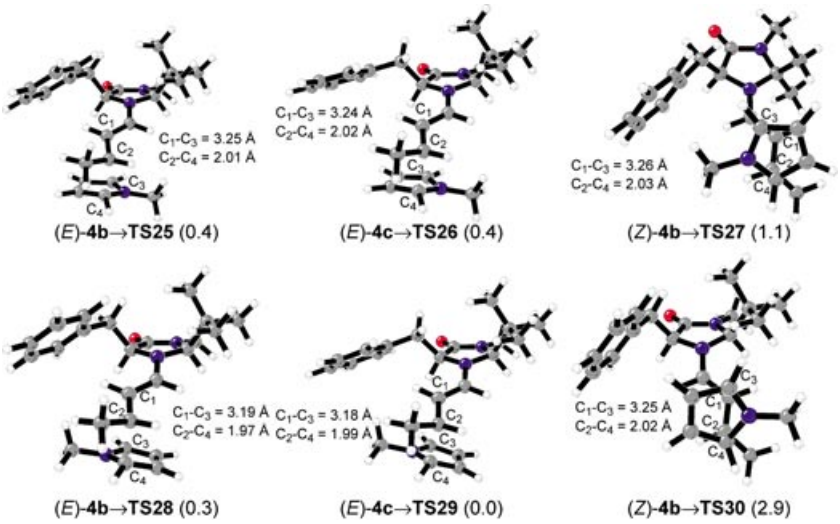

Figure 10. Optimized structures, relevant distances and relative energy difference for the most stable transition structures corresponding to *N*-methylpyrrole approach on the *exo*- and *endo*-(*Re*,*Si*)-face of iminium complex **4**.

In Figure 10, **TS25** – **TS30** correspond to closed-*exo* and closed-*endo* attack of *N*-methylpyrrole on the *Si*,*Re* face of iminium intermediate **4** (Figure 4). These lead to the compound isolated as the major enantiomer (Figure 7).[5] Even though (*E*)-**4c** is 0.7 kcal/mol higher in energy than (*E*)-**4b**, **TS25** and **TS26** are equal in energy. The lowest energy transition structure is the one where the *N*-methylpyrrole adopts the closed-*endo* orientation on the *Si*,*Re* face of eclipsed conformer **TS29**. However, the energy difference between the closed-*endo* and closed-*exo* orientations is small (0.4 kcal/mol). **TS28**, the closed-*endo* approach of *N*-methylpyrrole on the *Si*,*Re* face of the lowest energy conformer (*E*)-**4b** for iminium intermediate **4**, is only slightly higher in energy than **TS29** (0.3 kcal/mol).

The data of Figure 11, and the results listed in Table 5, show that attack on the *Re*,*Si* face of intermediate **4** leads to significantly higher energy transition states. The four possible approaches to conformer (*E*)-**4a** have large steric hindrance between one of the methyl groups of the *t*-butyl substituent and the phenyl ring of the benzyl group at position C5 of the imidazolidinone heterocycle.

Transition structures involving iminium intermediate (*Z*)-**4b** on the *Si*,*Re* face of the iminium intermediate (**TS27** and **TS30**) are always much higher in energy than the most stable one. For approach to the *Re*,*Si* face, **TS33** is equal in energy to **TS32** which corresponds to *N*-methylpyrrole attack on the "top-face" of (*E*)-**4b** conformer. **TS36**, which corresponds to "bottom-face" approach of pyrrole heterocycle to (*Z*)-**4b**, is 1.2 kcal/

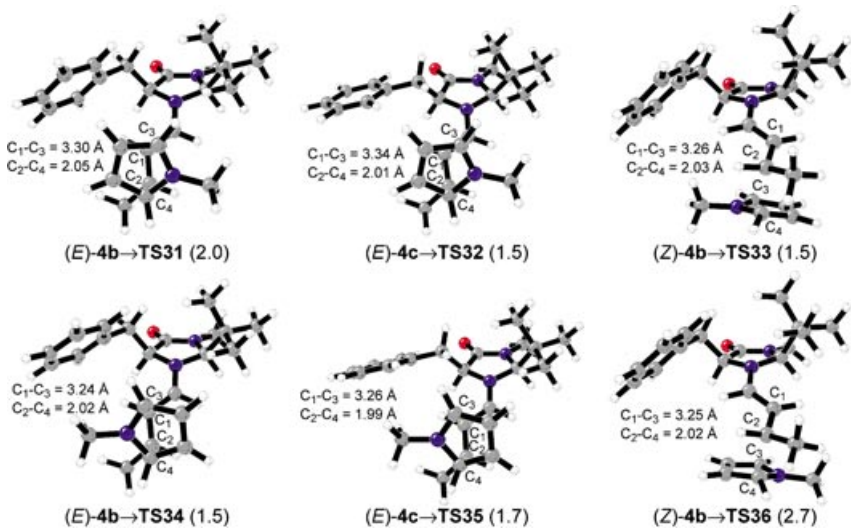

Figure 11. Optimized structures, relevant distances and relative energy difference for the most stable transition structures corresponding to *N*-methylpyrrole approach on the *exo*- and *endo*-(*Si*,*Re*)-face of iminium complex **4**.

mol higher in energy than the most stable *endo*-(*Re*,*Si*) transition structures **TS32**, **TS33**, and **TS34**.

A Boltzmann distribution gave a theoretical ee value of 90% for imidazolidinone **2** at $-60\,^{\circ}C$ in the gas phase versus 71% for catalyst **1**. Calculations predict a higher enantioselectivity for chiral amine **2** as was observed experimentally in the case of the alkylation reaction of *N*-methylindole with (*E*)-crotonaldehyde.[6] **TS25**, **TS26**, **TS28**, and **TS29** which correspond to closed-*exo* and -*endo* attack on (*Si*,*Re*) face of (*E*)-**4b** and (*E*)-**4c** iminium intermediates, and lead to the product isolated as major compound,[5] count for 92% of all the transition structures.

Tables 4 and 5 show that the energy differences between the attack on the two faces of the iminium intermediate are greater for catalyst **2**. The bulky *t*-butyl group effectively shields the *Re*,*Si* face of (*E*)-iminium intermediates. Since for both amine catalysts **1** and **2**, iminium ions (*Z*)-**3b** and (*Z*)-**4b** and the respective transition states count for only 4%, respectively, of the conformers at the reaction temperature, the observed enantioselectivities are closely connected with the percentage of (*E*)-**3b** or (*E*)-**4b** conformers. In both cases, the phenyl group hinders attack on the *Re*,*Si* face. Conformer (*E*)-**4b** is calculated to be the most stable conformation of intermediate **4**. It accounts for 81% of the intermediate formed in the gas phase at $-60\,^{\circ}C$. On the other hand, only 31% of conformer (*E*)-**3b** is formed for intermediate **3**. The higher percentage of conformer (*E*)-**4b** for intermediate **4** leads to higher enantioselectivity of the reaction. In addition, the most stable conformer for ion **3** is (*E*)-**3a**, which accounts for 53% of all the pos-

Table 5. Percentage of transition structures **TS29** – **TS44** in the gas phase at $-60\,^{\circ}C$.

Approach	Iminium Ion	Relative Energy [kcal/mol]	Percent
exo-(*Si*,*Re*)	(*E*)-**4a**	2.7	0
	(*E*)-**4b**	0.4	16
	(*E*)-**4c**	0.4	15
	(*Z*)-**4b**	1.1	3
endo-(*Si*,*Re*)	(*E*)-**4a**	3.1	0
	(*E*)-**4b**	0.3	21
	(*E*)-**4c**	0.0	40
	(*Z*)-**4b**	2.9	0
exo-(*Re*,*Si*)	(*E*)-**4a**	3.2	0
	(*E*)-**4b**	2.0	0
	(*E*)-**4c**	1.5	1
	(*Z*)-**4b**	1.5	1
endo-(*Re*,*Si*)	(*E*)-**4a**	4.1	0
	(*E*)-**4b**	1.5	1
	(*E*)-**4c**	1.7	1
	(*Z*)-**4b**	2.7	0

sible conformers. In this conformation, the phenyl group hinders attack on the *Re*,*Si* face to the least extent, as can be observed from the relatively low energies of transition structures **TS19** and **TS22**. MacMillan et al. pointed out that the *N*-methylpyrrole encounters a retarding interaction with the methyl substituent on the *Si*,*Re*, face of (*E*)-isomers as well.[6] The absence of this interaction in intermediate **4** leads to lower relative energy differences for attack on both alkene faces.

Results listed in Tables 4 and 5 show that the ratio of *exo*:*endo* orientations on *N*-methylpyrrole is 64:36 in the case of intermediate **3**. In contrast, the *exo*:*endo* ratio for intermediate **4** is 36:64. When comparing the four principle conformers, the same orientation is preferred for both intermediates. The reversal of the *exo*:*endo* ratio for intermediates **3** and **4** is due to the amount of each conformation present in the transition state. Conformation (*E*)-**3a**, which prefers *exo* orientation in both, *Si*,*Re* and *Re*,*Si* approaches, is more abundant in the transition state for intermediate **3**, while the transition state for intermediate **4** consists more of *endo* attack on *Si*,*Re* face of conformation (*E*)-**4c**. Thus, the *exo*:*endo* selectivity is essentially reversed. However, the small energy differences between the *endo* and *exo* orientations of each conformer demonstrate that a distinct preference for one over the other does not occur. This fact is in agreement with the experimental results obtained for the Diels–Alder reaction of cyclopentadiene and (*E*)-crotonaldehyde catalyzed by amine **1**, in which an 1:1 *endo*:*exo* ratio was observed.[3]

As pointed out previously in this paper (see Computational Methods section), only frequency calculations of the most stable transition structures corresponding to the reaction catalyzed by amine **1** were performed. The calculated energy difference between **TS13** and **TS16** including zero point vibrational energy correction is also 0.4 kcal/mol. We can conclude that inclusion of zero point vibrational energies are unlike to influence the calculated ee values to any large extent.

All the experiments were conducted in a THF-H_2O mixture. In order to check the solvent influence in the relative energy difference between the calculated transition structures, single point calculations of transition structures **13** and **16** were performed using the solvation model CPCM[17] and water as solvent. The obtained relative energy difference is 0.9 kcal/mol, *versus* 0.4 kcal/mol as the calculated value in the gas phase. This last result suggests that calculations performed with solvation correction should increase the relative energy differences between transition structures, and the calculated enantioselectivities.

Conclusion

The conformational analyses of intermediates **3** and **4** show that replacing the *gem*-dimethyl substituents on the catalyst framework for the *t*-butyl group changed the relative energies of the conformers. The lowest energy conformation for intermediate **3** places the phenyl ring away from the reactive site as a consequence of a stabilizing C–H$\cdots\pi$ interaction between one of the methyl groups at position C2 of the imidazolidinone ring and the phenyl ring of the benzyl group at position C5. This conformation is essentially avoided in intermediate **4** since the *t*-butyl group imposes additional steric hindrance. This leads to more effective shielding of the *Re*,*Si* face of (*E*)-intermediates yielding increased enantioselectivity of the reaction.

Acknowledgements

We are grateful to the National Institute of General Medical Sciences, National Institutes of Health for financial support of this research, and the National Computational Science Alliance, the National Science Foundation and UCLA Academic Technology Services for computer resources. R. G. thanks the Ministerio de Educación Cultura y Deporte-Spain for a postdoctoral fellowship. We thank Dr. Fernando R. Clemente for helpful discussions and suggestions.

References and Notes

[1] a) G. A. Olah, R. Krishnamurti, G. K. S. Prakash, in: *Comprehensive Organic Synthesis*, Vol. 3, (Ed.: I. Fleming), Pergamon Press, Oxford, **1991**, Chapter 1.8, pp. 293–339; b) R. M. Roberts, A. A. Khalaf, *Friedel–Crafts Alkylation Chemistry*, Marcel Dekker, New York, **1984**; c) *Friedel–Crafts Chemistry* (Ed.: G. A. Olah), Wiley, New York, **1973**; d) *Friedel–Crafts and Related Reactions*, Vols. 1–4, (Ed.: G. A. Olah), Wiley-Interscience, New York, **1963-1965**.

[2] a) N. Gathergood, W. Zhuang, K. A. Jorgensen, *J. Am. Chem. Soc.* **2000**, *122*, 12517–12522; b) S. Saaby, X. M. Fang, N. Gathergood, K. A. Jorgensen, *Angew. Chem. Int. Ed.* **2000**, *39*, 4114–4116; c) K. M. Jensen, J. Thorhauge, R. G. Hazell, K. A. Jørgensen *Angew. Chem. Int. Ed.* **2001**, *40*, 160–163.

[3] K. A. Kateri, C. J. Borths, D. W. C. MacMillan, *J. Am. Chem. Soc.* **2000**, *122*, 4243–4244.

[4] W. S. Jen, J. J. M. Wiener, D. W. C. MacMillan, *J. Am. Chem. Soc.* **2000**, *122*, 9874–9875.

[5] N. A. Paras, D. W. C. MacMillan, *J. Am. Chem. Soc.* **2001**, *123*, 4370–4371.

[6] J. F Austin, D. W. C. MacMillan, *J. Am. Chem. Soc.* **2002**, *124*, 1172–1173.

[7] N. A. Paras, D. W. C. MacMillan, *J. Am. Chem. Soc.* **2002**, *124*, 7894–7895.

[8] A. B. Northrup, D. W. C. MacMillan, *J. Am. Chem. Soc.* **2002**, *124*, 2458–2460.

[9] S. P. Brown, N. C. Goodwin, D. W. C. MacMillan, *J. Am. Chem. Soc.* **2003**, *125*, 1192–1194.

[10] S. P. Brown, M. P. Brochu, J. S. Sinz, D. W. C. MacMillan, *J. Am. Chem. Soc.* **2003**, *125*, 10808–10809.

[11] M. P. Brochu, S. P. Brown, D. W. C. MacMillan, *J. Am. Chem. Soc.* **2004**, *126*, ASAP article published in web on March 11th.
[12] Molecular mechanics conformational search, Monte Carlo simulation, MM3 force field; Macromodel V6.5.
[13] a) A. D. Becke, *J. Chem. Phys.* **1993**, *98*, 1372–1377; b) A. D. Becke, *J. Chem. Phys.* **1993**,*98*, 5648–5652; c) C. Lee, W. Yang, R. G. Parr, *Phys. Rev. B* **1988**, *37*, 785–789; d) R. Ditchfield, W. J. Hehre, J. A. Pople, *J. Chem. Phys.* **1971**, *54*, 724–728; e) W. J. Hehre, R. Ditchfield, J. A. Pople, *J. Chem. Phys.* **1972**, *56*, 2257–2261; f) P. C. Hariharan, J. A. Pople, *Theor. Chim. Acta* **1973**, *28*, 213–222.
[14] a) S. Bahmanyar, K. N. Houk, *J. Am. Chem. Soc.* **2001**, *123*, 11273–11283; b) L. Hoang, S. Bahmanyar, K. N. Houk, B. List, *J. Am. Chem. Soc.* **2003**, *125*, 16–17; c) S. Bahmanyar, K. N. Houk, H. J. Martin, B. List, *J. Am. Chem. Soc.* **2003**, *125*, 2475–2479; d) S. Bahmanyar, K. N. Houk, *Org. Lett.* **2003**, *5*, 1249–1251; e) G. Wayner, K. N. Houk, Y. K. Sun, *J. Am. Chem. Soc.* **2004**, *126*, 199–203.
[15] M. J. Frisch, G. W. Trucks, H. B. Schlegel, G. E. Scuseria, M. A. Robb, J. R. Cheeseman, V. G. Zakrzewski, J. A. Jr. Montgomery, R. E. Stratmann, J. C. Burant, S. Dapprich, J. M. Millam, A. D. Daniels, K. N. Kudin, M. C. Strain, O. Farkas, J. Tomasi, V. Barone, M. Cossi, R. Cammi, B. Mennucci, C. Pomelli, C. Adamo, S. Clifford, J. Ochterski, G. A. Petersson, P. Y. Ayala, Q. Cui, K. Morokuma, D. K. Malick, A. D. Rabuck, K. Raghavachari, J. B. Foresman, J. Cioslowski, J. V. Ortiz, B. B. Stefanov, G. Liu, A. Liashenko, P. Piskorz, I. R. Komaromi, R. Gomperts, L. Martin, D. J. Fox, T. Keith, M. A. Al-Laham, C. Y. Peng, A. Nanayakkara, C. Gonzalez, M. P. Challacombe, M. W. Gill, B. Johnson, W. Chen, M. W. Wong, J. L. Andres, C. Gonzalez, M. Head-Gordon, E. S. Replogle, J. A. Pople, *Gaussian 98*, revision A.6, Gaussian, Inc., Pittsburgh, PA, **1998**.
[16] A. P. Scott, L. Radom, *J. Phys. Chem.* **1996**, *100*, 16502–16513.
[17] a) B. Barone, M. Cossi, *J. Phys. Chem. A* **1998**, *102*, 1995–2001; b) B. Barone, M. Cossi, J. Tomasi, *J. Comput. Chem.* **1998**, *19*, 404–417.
[18] M. C. Kozlowski, M. Panda, *J. Org. Chem.* **2003**, *68*, 2061–2076.
[19] S. Tsuzuki, K. Honda, T. Uchimaru, M. Mikami, K. Tanabe, *J. Am. Chem. Soc.* **2000**, *122*, 3746–3753.
[20] a) G. Chalasinski, M. M. Szczesniak, *Chem. Rev.* **1994**, *94*, 1723–1765; b) S. Tsuzuki, T. Uchimaru, M. Mikami, K. Tanabe, *J. Phys. Chem. A* **1998**, *102*, 2091–2094; c) S. Tusuzuki, T. Uchimaru, K. Tanabe, *Chem. Phys. Lett.* **1998**, *287*, 202–208.
[21] a) C. Møller, M. S. Plesset, *Phys. Rev.* **1934**, *46*, 618–622; b) M. Head-Gordon, J. A. Pople, M. J. Frisch, *Chem. Phys.* Lett. **1988**, *153*, 503–506.
[22] R. Krishnan, J. S. Brinkley, R. Seeger, J. A. Pople, *J. Chem. Phys.* **1980**, *72*, 650–654.
[23] a) T. Clark, J. Chandrasekhar, G. W. Spitznagel, P. Von Ragué Schleyer, *J. Comput. Chem.* **1983**, *4*, 294–301; b) P. M. W. Gill, B. D. Johnson, J. A. Pople, M. J. Frisch, *Chem. Phys. Lett.* **1992**, *197*, 499–505; c) M. J. Frisch, J. A. Pople, J. S. Binkley, *J. Chem. Phys.* **1984**, *80*, 3265–3269.
[24] R. T. Morrison, R. N. Boyd, in: *Organic Chemistry*, 5th edn., Allyn and Bacon, Inc., Boston, **1987**, Chapters 14 and 35.
[25] Vibrational mode visualization was performed using the MOLDEN program: *Molden: a pre- and post-processing program for molecular and electronic structures*, G. Schaftenaar, J. H. Noordik, *J. Comput.-Aided Mol. Design* **2000**, *14*, 123–124.

